Evaluation of GAGG:Ce scintillators for future space applications

Published by IOP Publishing for Sissa Medialab
Received: *November 22, 2017*
Revised: *January 22, 2018*
Accepted: *February 5, 2018*
Published: *February 21, 2018*

Evaluation of GAGG:Ce scintillators for future space applications

M. Yoneyama,[a,1] **J. Kataoka,**[a] **M. Arimoto,**[a] **T. Masuda,**[a] **M. Yoshino,**[b,c] **K. Kamada,**[b,c] **A. Yoshikawa,**[b,c] **H. Sato**[d] **and Y. Usuki**[d]

[a] *Research Institute for Science and Engineering, Waseda University, 3-4-1 Okubo, Shinjyuku, Tokyo 169-8555, Japan*
[b] *Institute for Materials Research (IMR), Tohoku University, 2-2-1 Katahira, Aoba-ku, Sendai, Miyagi, 980-8577, Japan*
[c] *C & A Corporation, 6-6-40 Aoba, Aramaki, Aoba-ku, Sendai, Miyagi 980-8577, Japan*
[d] *Furukawa Scintitech Corporation, 1-25-13 Kannondai, Tsukuba, Ibaraki 305-0856, Japan*

E-mail: masaki-1047@akane.waseda.jp

Abstract: Cerium-doped $Gd_3(Ga, Al)_5O_{12}$ (GAGG:Ce) is a promising novel scintillator for gamma-ray detectors. While GAGG:Ce has already been implemented in various commercial products, its detailed characteristics and response to high-energy particles and gamma rays remain unknown. In particular, knowledge is lacking on the radiation tolerance of this scintillator against the gamma-ray and proton irradiation expected in future space satellite mission applications. In this study, we first investigate the light-yield energy dependence, energy resolution, decay time, radiation tolerance, and afterglow of GAGG:Ce scintillators under various temperature conditions. We find excellent linearity of ±3% between light yields and deposited energy over a wide range of 30–1836 keV; however, a light-yield deficit of more than 10% is observed below 30 keV of deposited gamma ray energy. We confirm that the temperature dependence of the light yield, energy resolution, and scintillation decay time is within 5–20% between −20 and 20 °C. We also evaluate the GAGG:Ce activation characteristics under proton irradiation and the light-yield degradation by accumulated dose using a ^{60}Co source. Moreover, we successfully identify various gamma-ray lines due to activation. Finally, we find a substantial afterglow for GAGG:Ce scintillators over a few hours; such an afterglow is only minimally observed in other scintillators such as CsI:Tl and $Bi_4Ge_3O_{12}$ (BGO). However, the afterglow can be substantially reduced through additional co-doping with divalent metal ions, such as Mg ions. These results suggest that GAGG:Ce is a promising scintillator with potential application in space satellite missions in the near future.

Keywords: Gamma detectors (scintillators, CZT, HPG, HgI etc); Scintillators, scintillation and light emission processes (solid, gas and liquid scintillators); X-ray detectors

[1] Corresponding author.

https://doi.org/10.1088/1748-0221/13/02/P02023

2018 JINST 13 P02023

Contents

1 Introduction

Scintillation detectors are widely used for spectroscopy and imaging. In particular, inorganic scintillators with high density and a high atomic number play an important role in the detection of high-energy gamma rays [1].

Recently, cerium-doped $Gd_3(Ga, Al)_5O_{12}$ (GAGG:Ce) [2] has been developed, which is a novel scintillator characterized by a high density (6.63 g/cm^3), high light yield (56,000 photon/MeV), fast scintillation decay time (~100 ns), and non-hygroscopicity. In addition, GAGG:Ce has an extremely low internal background; thus, it has been widely used in various applications related to high-energy astrophysics, molecular imaging for medical use, gamma-ray monitoring of environmental radioactive substances, etc. [3–10]. The major properties of GAGG:Ce and other typical inorganic scintillators (e.g., NaI:Tl, CsI:Tl, $Bi_4Ge_3O_{12}$(BGO), Gd_2SiO_5:Ce (GSO), etc.) are summarized in table 5 (appendix A).

2018 JINST 13 P02023

Various space missions have utilized scintillation detectors for X-ray and gamma-ray spectroscopy. NaI:Tl and CsI:Tl are most commonly used, particularly for low-earth-orbit (LEO) missions (e.g., the Compton Gamma Ray Observatory (CGRO) and the Rossi X-ray Timing Explorer (RXTE)) [11–13]. At LEO, however, high-energy charged particles, mostly protons, are trapped within local geomagnetic disturbances over Brazil; this is called the "South Atlantic Anomaly (SAA)". As satellites pass through the SAA several times per day, scintillation detectors are often "self-activated" through various nuclear reaction channels. In most cases, trapped protons having energies in the sub tens to hundreds of megaelectronvolt are the dominant source of activation, as they can pass through the satellite and detector shielding. Activation often causes significant degradation of detector performance, via the accumulation of long-lived activated atoms that increase the inherent detector background. In fact, significant increases in the detector background caused by activation have been reported for NaI:Tl and CsI:Tl [14, 15], occurring via the production of various radioactive daughters such as ^{123}I, ^{123}Te, and ^{125}I. Another problem affecting NaI:Tl and CsI:Tl is that the scintillator performance (e.g., energy resolution) degrades because of the absorbed radiation dose [16] and afterglow persistence for more than 1 ms [17–20].

In this context, BGO and GSO have attracted considerable attention as high-efficiency gamma-ray absorbers, which stems from their high density. They have been used in various applications such as medical systems (e.g., for positron emission tomography) [21–23] and X-ray detectors on board space satellites (e.g., Suzaku and the International Gamma-Ray Astrophysics Laboratory (INTEGRAL)) [24, 25]. Regarding activation characteristics, GSO has stronger tolerance to radiation than NaI:Tl and CsI:Tl [26–28], and BGO does not exhibit an afterglow [29]. Further, the light yield change of GSO due to the accumulated dose is small (10%) [30]. Because of these advantages, BGO and GSO have been widely used in space missions [24, 31–33]. However, BGO and GSO have several shortcomings: their light yields are approximately five times lower than that of NaI:Tl and have 30-50% temperature dependence [34, 35].

Although GAGG:Ce has recently been widely applied, only a small number of studies have been performed on this material, which have focused on limited topics for specific applications [36, 37]. In particular, the energy dependence of the light yield and the temperature characteristic, which are important for determining the GAGG:Ce performance, have not been investigated sufficiently.

In this study, we evaluate the basic characteristics of GAGG:Ce, including the radiation tolerance and afterglow, which are problematic in the context of space use. A comprehensive study of these characteristics would ensure the usefulness of GAGG:Ce for various applications. First, in section 2, we describe the basic performance of GAGG:Ce, considering its light yield and temperature characteristics. Then, we discuss the radiation tolerance for space application in section 3. In section 4, we report the results of afterglow investigations. Finally, we present relevant discussion and the conclusions of this study in section 5.

2 Basic performance

In this section, we report measurements of the various characteristics of GAGG:Ce scintillators relevant to spectroscopic applications. Hereafter, unless otherwise stated, "GAGG:Ce" refers to GAGG:Ce samples from Furukawa Co., having dimensions of 5×5×5 mm^3 (figure 1).

2018 JINST 13 P02023

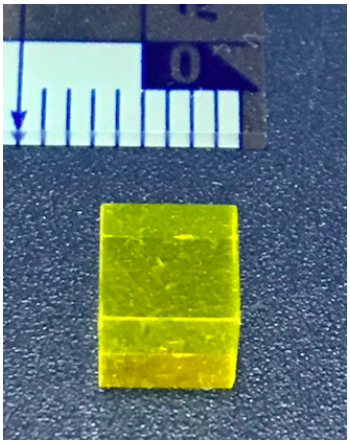

Figure 1. GAGG:Ce scintillator (5×5×5 mm^3).

2.1 Light-yield energy dependence

In order to measure the light-yield energy dependence, we obtained energy spectra using different radioisotopes by attaching the GAGG:Ce sample to a photo multiplier tube (PMT; Super Bialkali R3998-100-02HA, Hamamatsu).

Both the GAGG:Ce and PMT were placed in a thermostatic chamber. The operation temperature was set to 20±1 °C. A schematic of the experimental setup is shown in figure 2. The GAGG:Ce was covered with an enhanced specular reflector (ESR) sheet (inside) and teflon tape (outside) as a reflector. The output signal from the PMT was transmitted to a preamplifier (CP506E, Clear Pulse) and then shaped by a shaper (Model 570, Ortec) for a shaping time of 10 µs. A digital multichannel analyzer (MCA8000D) digitalized the shaped pulse heights, yielding digital values (MCA channel) that were sent to a personal computer (PC). Radioactive sources (^{109}Cd, ^{133}Ba, ^{241}Am, ^{57}Co, ^{22}Na, ^{137}Cs, ^{54}Mn, ^{60}Co, and ^{88}Y source) with emissions of 22 to 1836 keV were used in our measurement. Using a test-pulse signal, the integral non-linearity (INL) of our measurement system without the scintillator and PMT was estimated to be approximately 0.001%. Since the dynamic range of input test-pulse was 2.4 MeV for GAGG:Ce and 3.2 MeV for CsI:Tl, INL of 0.001% corresponds to the equivalent energy range of ~30 eV.

The pulse heights of the gamma-ray events obtained from GAGG:Ce and CsI:Tl using the various radioactive sources are shown in figure 3. Here, we estimated the photopeaks by the Gaussian fit. After correcting the non-linearity relationship of our measurement system without scintillators, we fit the experimental data with a linear function.

The residuals of GAGG:Ce and CsI:Tl from the best-fit function are shown in figure 4. While there is a good linear relation in GAGG:Ce from 30 to 1836 keV within the residual of 3%, there exists a significant degradation (>10%) below 30 keV, indicating substantial decrease of light yield at such low energy. In contrast, the residuals of CsI:Tl are less than approximately 5%, within the energy range of 22 to 1836 keV.

The energy resolution (full width at half maximum; FWHM) of the GAGG:Ce and CsI:Tl at 20 °C are shown as a function of gamma-ray energy in figure 5. The best-fit function of GAGG:Ce and CsI:Tl are proportional to $E^{-0.475\pm0.002}$ and $E^{-0.428\pm0.001}$ respectively, both of which are almost

2018 JINST 13 P02023

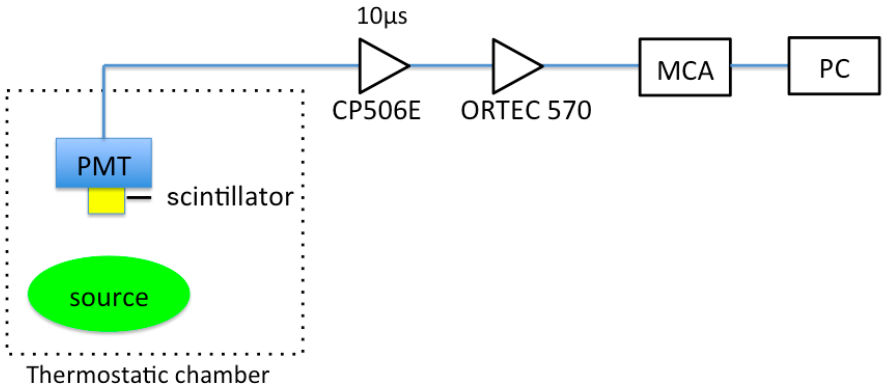

Figure 2. Measurement setup to determine light-yield energy dependence.

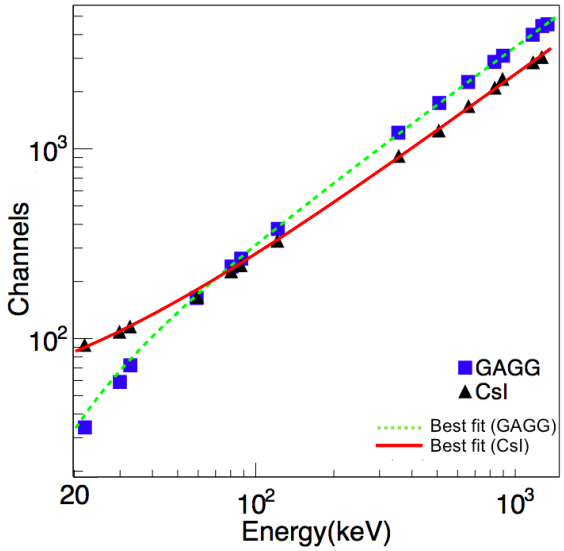

Figure 3. GAGG:Ce and CsI:Tl light yield dependence on gamma-ray energy (dashed and solid lines: best-fit linear functions).

consistent with the ideal index of −0.5 determined from the photon statistics considering the photo electron numbers.

2.2 Temperature dependence

2.2.1 Light yield and energy resolution

The experimental setup for measurement of the temperature dependence of the light yield and energy resolution (figure 2) was identical to that of the linearity measurement described in section 2.1, except the GAGG:Ce was coupled to a multi-pixel photon counter (MPPC) (50 μm pitch, 3×3 mm^2; Hamamatsu). The light yield and energy resolution of the GAGG:Ce depending on temperature were obtained for a ^{137}Cs source (662 keV) in the temperature range of −45 to 45 °C. Note that the temperature variation of the MPPC gain was measured prior to this experiment and appropriate corrections were subsequently made.

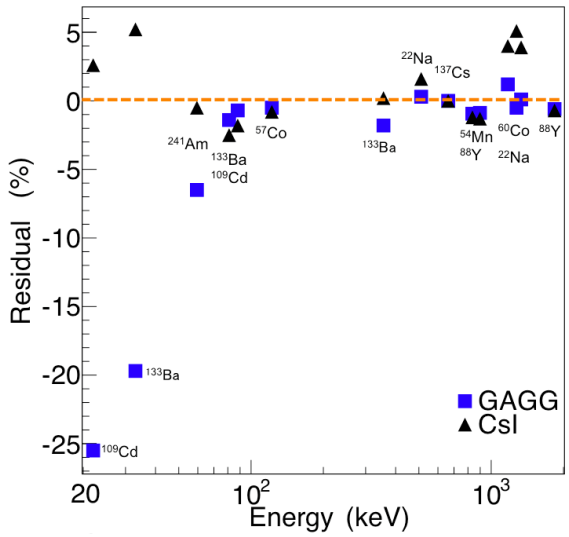

Figure 4. Residuals of light-yield energy dependence normalized at 662 keV (dashed line: 0% residual).

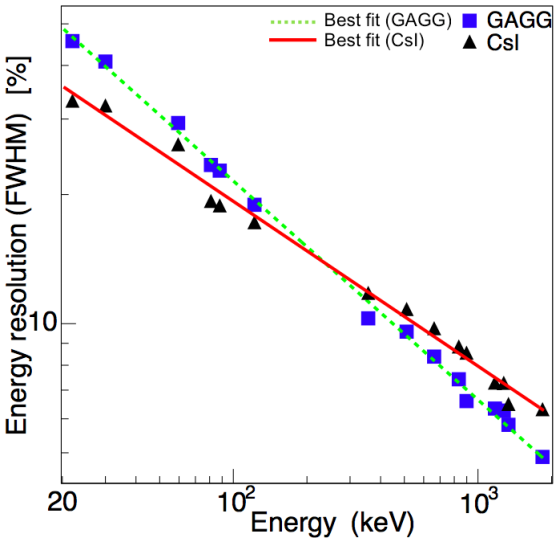

Figure 5. Energy resolutions of GAGG:Ce and CsI:Tl (dashed and solid lines: best-fit power-law functions of GAGG:Ce and CsI:Tl, respectively).

The temperature dependence of the light yield and energy resolution is shown in figures 6 and 7, respectively. For the results shown in figure 6, the vertical values were normalized at room temperature (20 °C) to 1. The optimal light yield and energy resolution appear at −20 °C. The temperature dependence of the GAGG:Ce light yield (20%) is less than that of BGO [34] (for light yields between −20 and 20 °C, the typical temperature dependence of BGO is 50%).

2.2.2 Scintillation decay time

We obtained the scintillation decay time of GAGG:Ce as a function of temperature. The GAGG:Ce waveform of gamma-rays from the ^{137}Cs source through the PMT was acquired using an oscillo-

2018 JINST 13 P02023

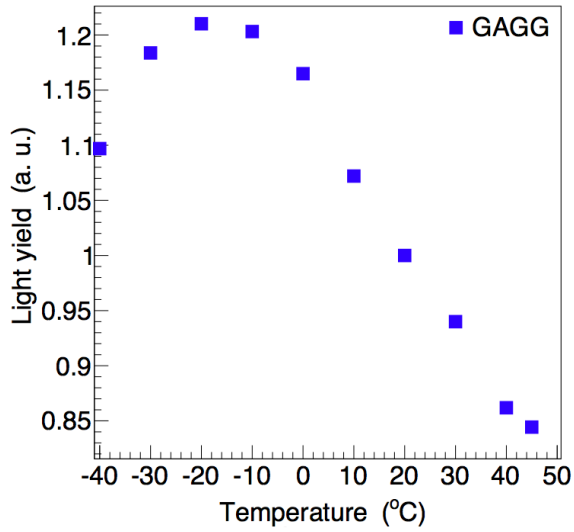

Figure 6. Light yield of GAGG:Ce as function of temperature (normalized light yield at 20 °C).

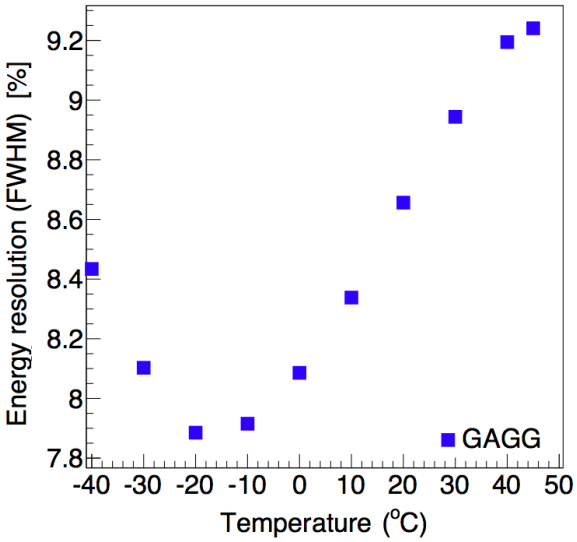

Figure 7. Energy resolution of GAGG:Ce as function of temperature.

scope. The experimental setup for the scintillation decay time measurement is shown in figure 8. A single exponential function was adopted and the scintillation decay time was estimated. The experiment was performed for a temperature range of −40 to 40 °C.

We evaluated the temperature dependence of the scintillation decay time. The waveforms obtained through measurement were fitted and well determined by a single exponential function at each temperature (figure 9).

At room temperature (20 °C), a scintillation decay time of 98.4 ns is obtained, as shown in figure 10. As the temperature decreases, the scintillation decay times increase. For example, at −40 °C, the scintillation decay time is 106.4 ns. For GAGG:Ce, the decay time change between −40 and 40 °C is ∼12% (figure 10), while that of CsI:Tl is ∼50% [38]. For NaI, the decay time changes by a factor of ∼40% between −40 and 40 °C [39].

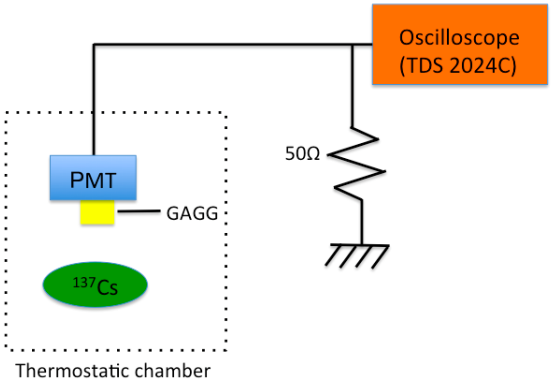

Figure 8. Experimental setup for measurement of scintillation decay time.

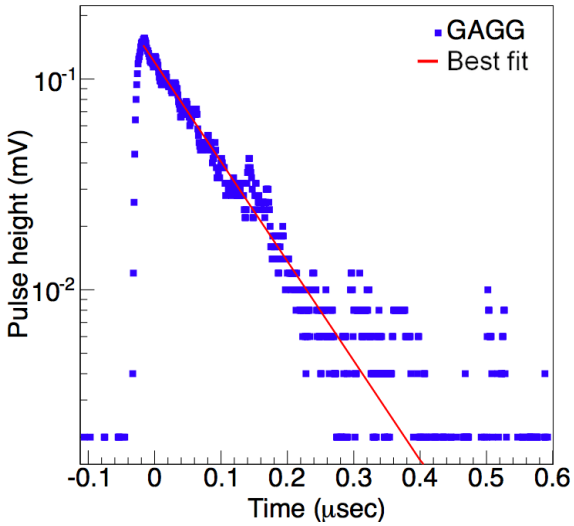

Figure 9. An example of scintillation decay time of GAGG:Ce at 20 °C (solid line: best-fit single exponential function).

3 Radiation tolerance

3.1 Activation

We irradiated the GAGG:Ce sample (20×20×2 mm^3) with 10 krad (equivalent to ~10 years' exposure, 1.25×10^{11} protons/cm^2) using 70-MeV protons provided by the ring cyclotron facility at the National Institute for Quantum and Radiological Sciences and Technology, Japan. The GAGG:Ce activation spectrum produced by the proton was measured using a high-purity Ge detector (GC3018, Canberra) (figure 11). Irradiation condition was as follows: GAGG:Ce was placed in the dark at environmental temperature of 15 °C.

The activation spectra of GAGG:Ce obtained over different time periods are shown in figure 12. We confirmed a pair annihilation line (511 keV) from the β^+ decays of Gd and fluorescence gamma-ray lines (e.g., 102.5, 220.1, 333.3, 629.5, 784.4, 871.4, 993.7, and 1038.2 keV) possibly originating from Gd, Ga, Tb (Gd daughter), and Eu (Gd daughter). We could identify radioactive isotopes

2018 JINST 13 P02023

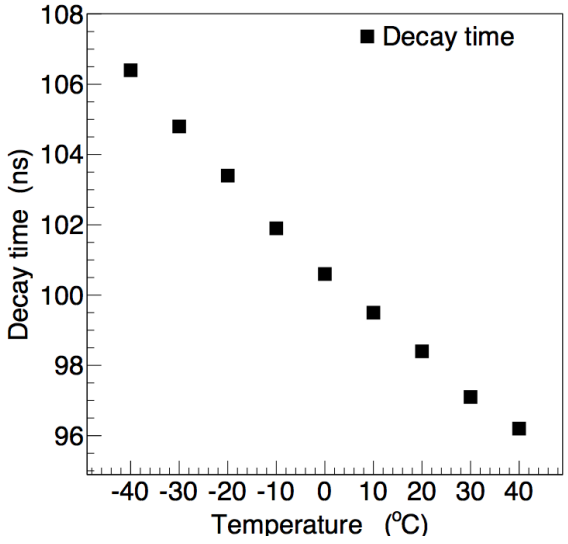

Figure 10. Temperature dependence of GAGG:Ce scintillation decay times.

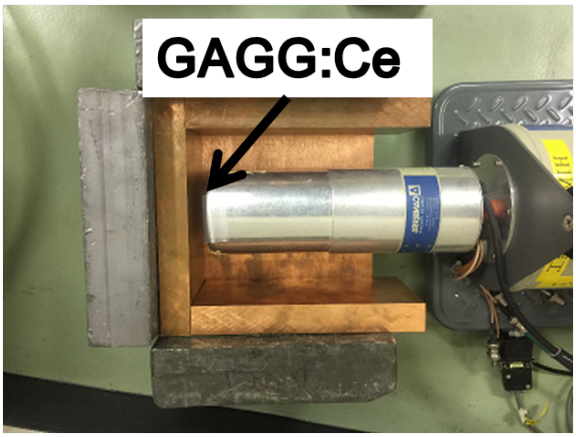

Figure 11. Ge detector for activation characteristic measurement.

produced through proton nuclear reaction (table 1); those with significant 2σ or more are listed in table 1. Note that a prominent line is apparent at 511 keV, indicating that GAGG:Ce is not suitable for the 511-keV survey frequently performed in space missions [40, 41].

Regarding the continuum component, we compared the GAGG:Ce data with those for BGO and GSO between 30 and 600 keV [26] (figure 13). Note that BGO and GSO were selected for comparison here because they have been successfully used in the space environment. The activated background rate of GAGG:Ce is 10^{-8} counts/s/cm^3/protons soon after proton beam irradiation; this decreases as a function of $t^{-0.82\pm0.02}$. Note that the differences in detector sensitivity, experiment geometry, and proton beam energy and shape were not perfectly corrected. Thus, figure 13 presents a very rough comparison only. A similar study on the activation background of GAGG:Ce has been performed previously [27], and the results are almost consistent with those of our study; however, the observed fluxes differ slightly, by a factor of 2. This inconsistency is due to differences in

2018 JINST 13 P02023

Table 1. Identified radioactive isotopes (the error of the upper limit is 2σ; otherwise, the error is 1σ).

Energy [keV]	Radioactive isotopes	Half life (experiment) [min]	Half life (literature) [min]	Significance (σ)
102.5	^{159}Eu, ^{150}Tb	6.9 ± 3.2	18.1, 5.8	3.4
	^{154}Eu	72.8 ± 50.3	46.0	3.4
220.1	^{152}Tb	8.4 ± 1.1	4.2	3.2
333.3	^{144}Gd	6.9 ± 3.2	4.4	4.5
511	pair annihilation line	14.0 ± 3.0	–	21.8
	pair annihilation line	82.0 ± 13.1	–	21.8
629.5	^{148}Tb, ^{149}Tb, ^{152}Tb	8.9 ± 1.3	5.8, 4.2, 4.2	7.2
784.4	^{148}Tb	7.2 ± 1.8	5.8, 4.2	6.1
871.4	^{65}Ga	10.7 ± 3.3	15.2	5.6
993.7	^{65}Ga	<63.5 (upper limit)	15.2	2.0
1038.2	^{159}Eu	<135.4 (upper limit)	18.1	2.0

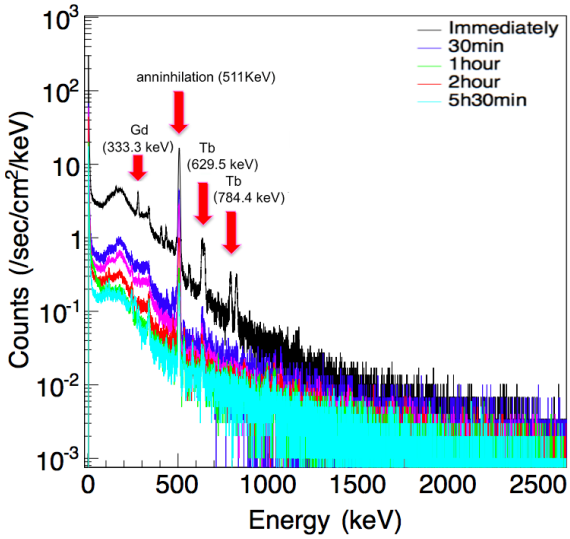

Figure 12. Activation spectra of GAGG:Ce after proton irradiation.

the employed detector, its geometry, the proton beam energy, and the GAGG:Ce sample. Thus, this activation background result for GAGG:Ce is considered to be consistent with the findings of previous studies. Furthermore, based on the result of the activation background, we calculated a temporal change of the inherent detector background caused by activation of GAGG:Ce in the LEO (figure 24, appendix B).

The half-lives of the distinctive lines obtained in this study were estimated from the temporal evolution of the line flux and compared with the values in the literature [42, 43]. Detailed results for the fitted temporal evolution of the identified lines are presented in appendix C. Hence, we found that the obtained half-lives of the distinctive lines are almost consistent with the half-lives reported in the literature, as apparent from table 1. These half-life results strongly support the previous argument based on line identification from our spectroscopy.

2018 JINST 13 P02023

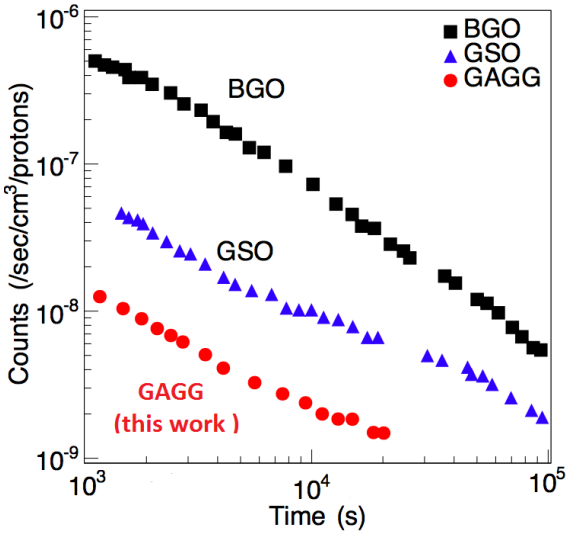

Figure 13. GAGG:Ce activation background compared with those for GSO and BGO, calculated from continuum components from 30 to 600 keV.

3.2 Light-yield degradation from accumulated dose test

We irradiated a GAGG:Ce sample for a 100-krad dose at the ^{60}Co irradiation facility at the Tokyo Institute of Technology, Japan. Although ^{60}Co emits 1170- and 1332-keV gamma rays, Compton scattered electrons as well as bremsstrahlung X-rays emitted from sub-MeV electorns are major sources of a radiation dose, which mimics the space environment [44, 45]. For example, a 100-krad dose corresponds to approximately 100 years of space application in a typical LEO [46]. We irradiated the GAGG:Ce sample in the dark at environmental temperature of 22 °C. For comparison with the GAGG:Ce, BGO was also irradiated under the same conditions. Before and after the ^{60}Co irradiation, we obtained X-ray spectra using a ^{109}Cd source, so as to evaluate the light yield. The experiment for obtaining the X-ray spectra was performed in a thermostatic chamber, with the temperature maintained at 20 °C. The details of the experimental setup are identical to those for measurement of the light-yield temperature dependence described in section 2.2.1.

The spectra obtained before and after the ^{60}Co irradiation are shown in figure 14. The peak positions for the ^{109}Cd (22 and 88 keV) before and after the ^{60}Co irradiation differ by ~10%, as summarized in table 2. Thus, we confirmed that the light-yield degradation due to a 100-krad ^{60}Co source is small in GAGG:Ce (~10%). In CsI:Tl, irradiation with a 100-krad dose from a ^{60}Co source was found to degrade the light yield by 20–70% [47]. For BGO, the light yield decreased by ~15% in our experiment (table 1); this is consistent with the findings of a previous study (10–40% [48]).

4 Afterglow

4.1 Temporal characteristic

The measurement setup for the afterglow investigation is shown in figure 15. We placed the GAGG:Ce sample in a thermostatic chamber that maintained the temperature at 20 °C. Following irradiation with blue light-emitting-diode (LED) light (471 nm) for 30 s, the MPPC current was

2018 JINST 13 P02023

Table 2. Peak positions and energy resolutions of GAGG:Ce and BGO for ^{109}Cd source before and after ^{60}Co irradiation.

GAGG:Ce	Peak position (22 keV) [ch]	Peak position (88 keV) [ch]	Energy resolution (FWHM) (22 keV) [%]	Energy resolution (FWHM) (88 keV) [%]
Before irradiation	567.3 ± 0.3	2513.9 ± 1.3	43.1 ± 0.1	23.0 ± 0.2
After irradiation[1]	519.9 ± 0.3	2309.0 ± 1.2	44.0 ± 0.2	23.6 ± 0.2
BGO	Peak position (22 keV) [ch]	Peak position (88 keV) [ch]	Energy resolution (FWHM) (22 keV) [%]	Energy resolution (FWHM) (88 keV) [%]
Before irradiation	326.3 ± 0.5	1512.9 ± 1.2	69.6 ± 0.2	33.3 ± 0.2
After irradiation[1]	285.1 ± 0.5	1324.2 ± 1.2	71.0 ± 0.1	35.1 ± 0.1

[1]The measurement was performed one day after irradiation.

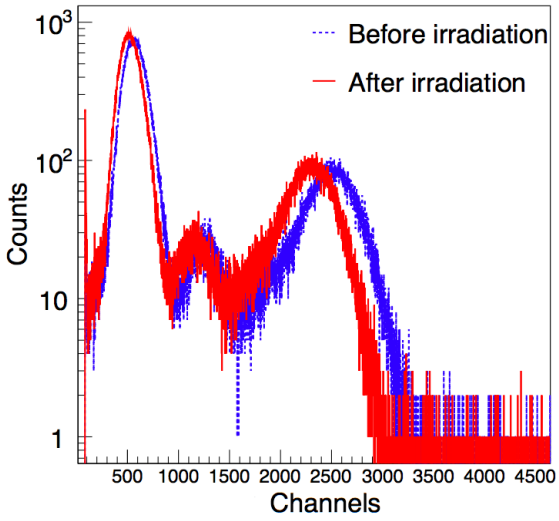

Figure 14. GAGG:Ce spectra for ^{109}Cd source before and after ^{60}Co irradiation.

measured as the GAGG:Ce afterglow. Note that the LED was placed not to irradiate the photosensitive area of the MPPC. Also, we used a small MPPC instead of the PMT, because the measurement system had to be integrated with the LED and put in a small thermostatic chamber. We performed similar measurements using BGO, CsI:Tl, $Y_3Al_5O_{12}$ (yttrium aluminum garnet; YAG), $Lu_3Al_5O_{12}$ (LuAG), and $Lu_{1.8}Y_{0.2}SiO_5$ (LYSO) scintillators for comparison.

As the characteristics of the GAGG:Ce afterglow have never been studied, we systematically measured this behavior and compared the results with those for other scintillators (BGO, CsI, YAG, LuAG, and LYSO). The detector response as indicated by the MPPC gain and the LED light intensity were considered. Figure 16 shows the afterglow results for GAGG:Ce and other scintillators irradiated by LED light at 471 nm. In this study, the afterglow rate is defined as the ratio of the current value for the afterglow after LED deactivation to the current value during LED irradiation. In general, it is known that LED light itself has afterglow, which continues after few tens of seconds even after the LED light is turned off. Therefore, we performed similar measurement by using the MPPC and LED light without scintillators to understand the afterglow performance

2018 JINST 13 P02023

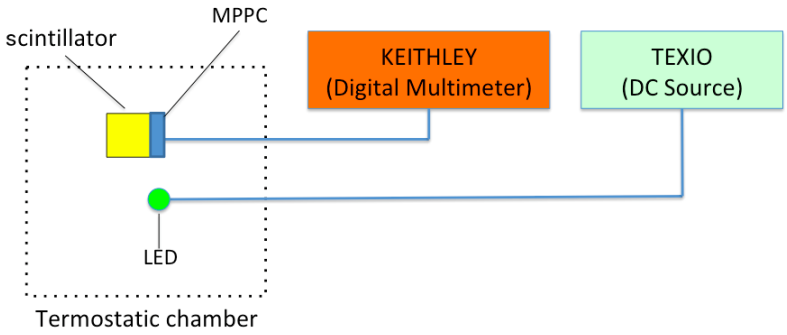

Figure 15. Setup for afterglow measurement.

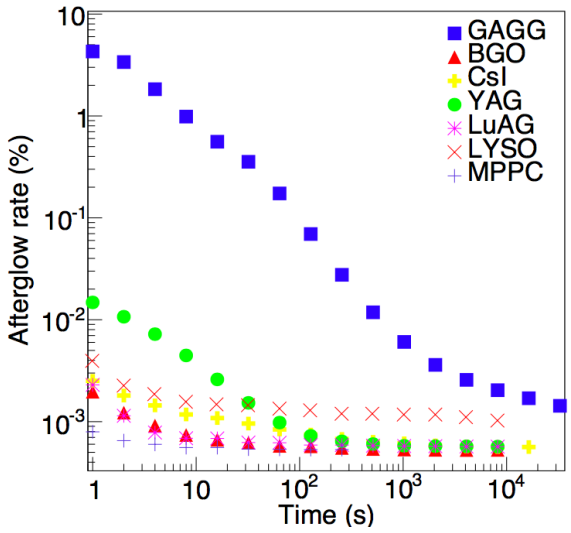

Figure 16. GAGG:Ce afterglow compared with those of other scintillators.

of the LED light after turning off the LED light. We found that the afterglow of LED light lasted for approximately 10 s. This is the reason for apparent temporal variation of current value for measurements of BGO, CsI:Tl, LuAG, and LYSO in the first 10 s (figure 16). Note that GAGG:Ce has much larger afterglow than LED light and the largest afterglow rate (~4% 1 s after the LED deactivation) among the examined scintillators. Even 1 hour after irradiation, the afterglow of GAGG:Ce is considerably larger than those of the other scintillators.

Similar behavior is apparent for YAG; however, the afterglow rate of YAG is considerably smaller than that of GAGG:Ce, i.e., by two orders of magnitude. The GAGG:Ce afterglow rate appears to be relatively shallow in the first few tens of seconds, but the trendline becomes steep about 100 s after irradiation, indicating that the trend has two components. These components may be caused by two of three traps: deep traps due to O^{2-} defects [49–51], deep traps due to cation defects during crystal growth [50, 52], and shallow traps due to antisite defects [50, 53]. Figure 16 shows that the GAGG:Ce afterglow decreases with time: $t^{-1.24\pm0.01}$ (100–1,000 s) and $t^{-0.26\pm0.02}$ (1,000–32,000 s). These observations are consistent with the time scale of the afterglow component (several hours) reported in a previous study [54].

2018 JINST 13 P02023

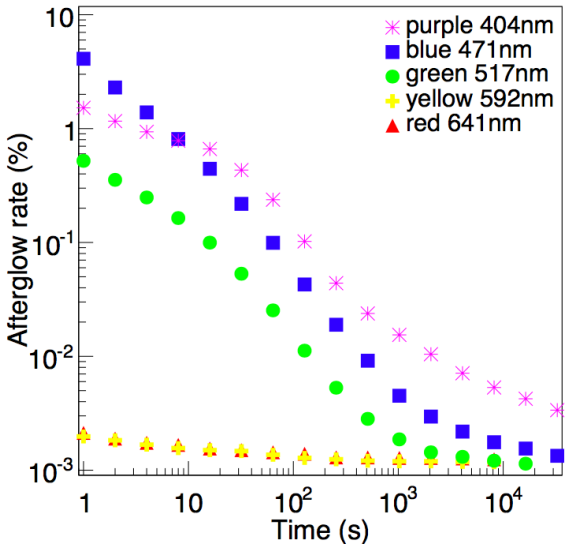

Figure 17. GAGG:Ce afterglow for different wavelength LEDs.

4.2 Dependence on light irradiation wavelength

In order to evaluate the emission-wavelength dependence of the afterglow, we irradiated scintillators with the different-wavelength LEDs: purple (404 nm), blue (471 nm), green (517 nm), yellow (592 nm), and red (641 nm) LED light for 30 s, using the setup shown in figure 15.

Figure 17 shows the afterglow wavelength dependence obtained using these different LED lights. It is apparent that irradiation with purple (404 nm), blue (471 nm), and green (517 nm) LED light causes an afterglow. The obtained results are in accordance with the results obtained from detailed spectroscopy of the afterglow emission in section 4.6.

4.3 Influence of afterglow on energy resolution

The afterglow is expected to affect the spectroscopy accuracy significantly. Therefore, we evaluated this effect by obtaining ^{137}Cs spectra after LED irradiation for 30 s. The measurement was performed immediately after the LED light (471 nm) was deactivated. The experimental setup is shown in figure 2.

During the initial 100 s, the afterglow contributes to 1% degradation of the energy resolution (figure 18). After 400 s, the energy resolution becomes almost constant. Note that the difference in energy resolution between figures 7 and 18 is caused by the different detectors (MPPC and PMT for the data in figures 7 and 18, respectively).

4.4 Temperature dependence of afterglow

In order to evaluate temperature dependence of afterglow, an afterglow measurement was performed by changing the temperature between 0 and 20 °C and with a blue LED light (471 nm) irradiation for 30 s, again using the setup shown in figure 15.

The results indicating the afterglow temperature dependence are shown in figure 19, for which the temperature dependence of the MPPC gain and the LED light intensity are corrected. We found

2018 JINST 13 P02023

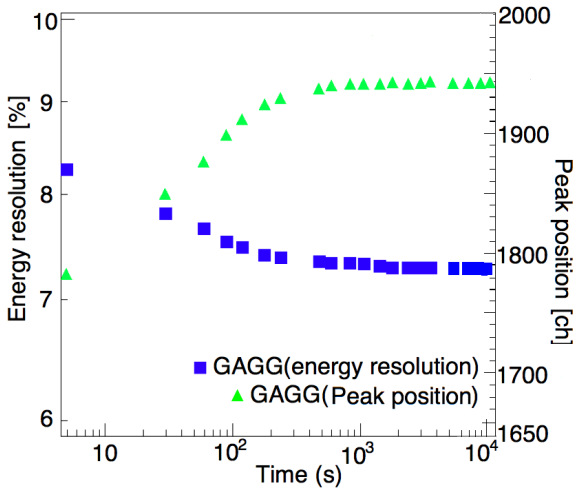

Figure 18. Influence of afterglow on energy resolution (FWHM) for ^{137}Cs (662 keV).

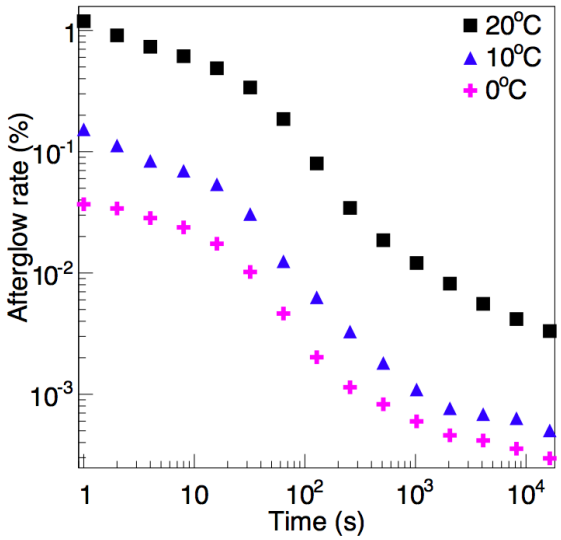

Figure 19. Temperature dependence of GAGG:Ce afterglow.

that the afterglow increases with increasing temperature. It is conceivable that electrons caught in a trap of afterglow generation are released at high temperature. Thus, when the temperature increases, the number of excited electrons (i.e., afterglow) also increases.

4.5 Afterglow due to electron and gamma-ray irradiation

As mentioned in section 3.2, substantial amount of high-energy electorns in space environment will degrade the light-yield of GAGG:Ce scintillators. Moreover, such large amount of energy deposit by electrons may cause similar afterglow as has been observed in the LED light discussed in section 4.1. In order to evaluate the afterglow of GAGG:Ce due to accumulation electron and gamma-ray dose, we irradiated GAGG:Ce with a 100-krad dose (figure 20) from a ^{60}Co source in the dark at 22 °C. The irradiation was already performed as described in section 3.2. We replaced GAGG:Ce with BGO and

2018 JINST 13 P02023

Table 3. Afterglow current values of GAGG:Ce and BGO before and after ^{60}Co irradiation.

	GAGG:Ce	BGO
Before irradiation	0.25 ± 0.01 μA	0.14 ± 0.01 μA
After irradiation[1]	23.27 ± 0.01 μA	0.15 ± 0.01 μA

[1]The measurements were performed 300 s after irradiation.

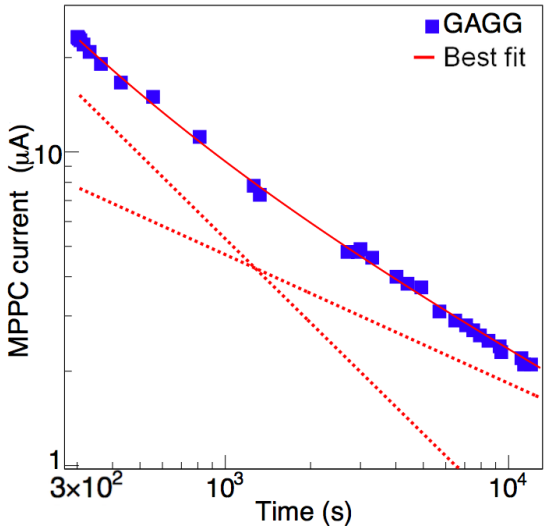

Figure 20. Afterglow current of GAGG:Ce irradiated by ^{60}Co source (dashed lines: best-fit power-law functions, solid line: the sum of the two functions).

performed the same irradiation test. Hence, we confirmed that GAGG:Ce emits an afterglow with a long decay time (several days). On the other hand, BGO does not exhibit a significant long-term afterglow component (table 3); this is consistent with the findings mentioned in section 4.1.

Figure 20 shows that the GAGG:Ce afterglow current decreases with time: $t^{-1.25\pm0.08}$ (300–1,000 s) and $t^{-0.50\pm0.02}$ (1,000–12,000 s). The attenuation owing to the function of $t^{-1.25}$ is consistent with that obtained for LED illumination, as described in section 4.1. This result indicates that the afterglows owing to LED irradiation and to electron and gamma-ray irradiation are caused by a similar process. On the other hand, after 1,000 s, the power-law index of the afterglow owing to the ^{60}Co source (−0.50) is slightly different from that owing to the LED irradiation (−0.25). This difference might be due to the difference between the radioluminescence (^{60}Co source) and the photoluminescence (LED light).

4.6 Emission spectra of afterglow, photoluminescence, and radioluminescence

The most serious problem impeding use of GAGG:Ce is the afterglow. Therefore, we investigated a method of decreasing the afterglow. Although we showed the wavelength dependence of the afterglow emission in section 4.2, the measurement accuracy of the afterglow emission wavelength may be too poor (potential error: 50–100 nm) to elucidate the afterglow origin. Therefore, we performed detailed spectroscopy of both the afterglow and prompt photoluminescence in the dark at 24 °C (during 440 nm LED illumination for approximately 10 s) using the fluorescence spectrophotome-

2018 JINST 13 P02023

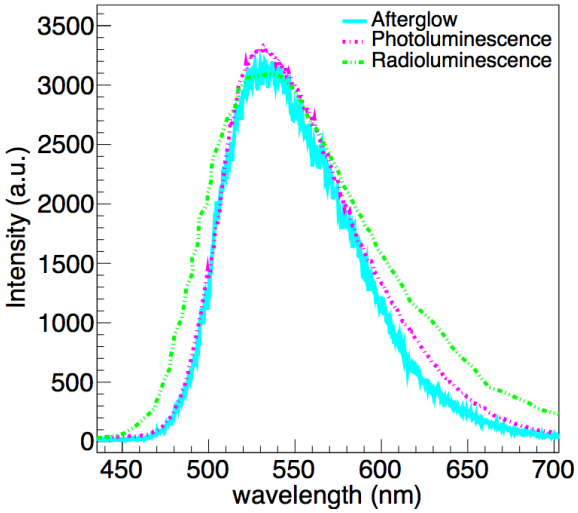

Figure 21. Emission spectra of GAGG:Ce afterglow, photoluminescence (excitation wave length: 440 nm), and radio luminescence [58].

Table 4. GAGG:Ce sample composition and scintillation light yield.

GAGG:Ce	Composition	Peak position for 662 keV (normalized at Non-doped)	Energy resolution (FWHM) for 662 keV
Non-doped	$Gd_3Ga_3Al_2O_{12}$: Ce, Mg : 0 ppm	1.00	7.58%
Sample 1	$Gd_3Ga_{2.4}Al_{2.6}O_{12}$: Ce, Mg : 1,000 ppm	0.70	9.42%
Sample 2	$Gd_3Ga_3Al_2O_{12}$: Ce, Mg : 2,000 ppm	0.48	14.42%

ter (F-4500, HITACHI). The obtained emission spectra for the GAGG:Ce afterglow and prompt photoluminescence are shown in figure 21. It is apparent that both peak values are consistently approximately 530 nm. As regards the afterglow origin, light emission may occur as a result of the electron-hole recombination at the 4f level, similar to photoluminescence and radioluminescence. As the 4f-5d_1 and 4f-5d_2 level transitions [55, 56] are fast [57], it is suggested that a trap causing the afterglow is located somewhere different to this level. These features are helpful for elucidating the afterglow process.

4.7 Improvement of afterglow by co-doping with Mg

Recent studies have reported that scintillation light yield decreases when the scintillator is co-doped with divalent metal ions; however, the scintillation decay time is shortened [59, 60]. Therefore, we aimed to reduce the afterglow by co-doping with Mg, a divalent metal ion. We adjusted the GAGG:Ce composition as detailed in table 4.

We fabricated three GAGG:Ce samples with different Mg doping fractions, labeled Samples 1 (Mg : 1,000 ppm) and 2 (Mg : 2,000 ppm), and Non-doped GAGG:Ce (Mg : 0 ppm). The setup used to measure the afterglow is shown in figure 15.

2018 JINST 13 P02023

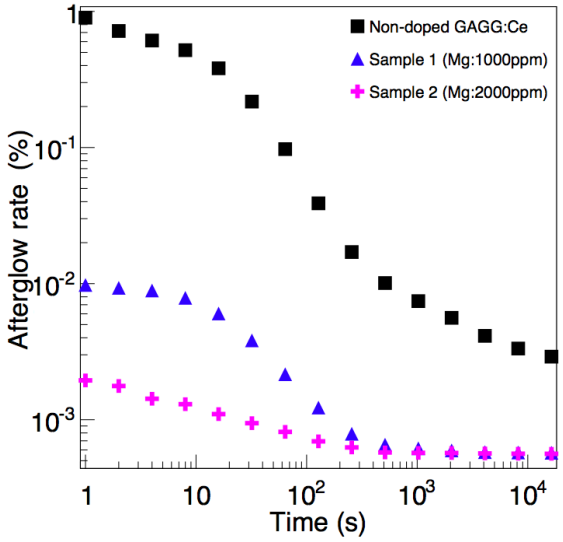

Figure 22. Afterglows of Mg-doped GAGG:Ce samples for LED irradiation.

The three samples were irradiated with LED light (471 nm) 30 s and the results are shown in figure 22. From this figure, it is apparent that the afterglow decay times for Samples 1 and 2 are approximately 100 s, and the afterglow light amount of these samples are lower than that of the Non-doped GAGG:Ce sample by several orders of magnitude. Thus, dramatic afterglow reduction was obtained for Samples 1 and 2 through doping with Mg. As the Shannon radius of the Mg ion is comparatively close to those of Al and Gd ions, Mg may compensate for Ga defect traps [49], yielding a decrease in the afterglow. However, the scintillation light yields for Samples 1 and 2 are 1.5–2 times smaller than that of the Non-doped GAGG:Ce, as shown in figure 23. We note that, even if the scintillation light yield is decreased through Mg doping, it remains 3–4 times larger than those of BGO and GSO (table 5, appendix A).

5 Discussion and conclusion

We have measured the GAGG:Ce light-yield dependence on the incident gamma-ray energy and temperature, the decay-time dependence on temperature, and the radiation tolerance. For the radiation tolerance, we estimated the activation characteristic using a proton beam and the light-yield degradation due to a 100-krad dose from a ^{60}Co source. Furthermore, we have reported the first measurements of strong GAGG:Ce afterglow through comparison with other scintillators and discussed the afterglow characteristic, which depends on the wavelength of the light irradiating the GAGG:Ce.

The advantages and disadvantages of GAGG:Ce are briefly summarized below.

1. Advantages

   - The light-yield temperature dependence is small (20% between −20 and 20 °C)
   - The decay-time temperature dependence is small (10% between −40 and 40 °C)
   - The activation background rate is small (10^{-8} counts/s/cm^3/protons immediately after irradiation)
   - The light-yield degradation due to a 100-krad dose is small (~10%)

2018 JINST 13 P02023

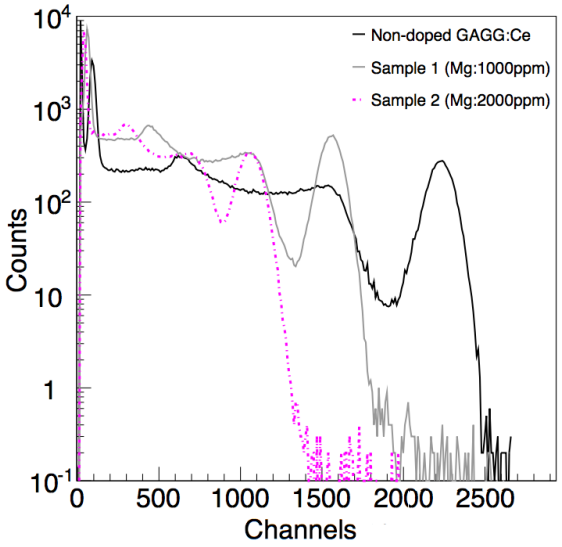

Figure 23. Spectra of three GAGG:Ce samples for ^{137}Cs source.

2. Disadvantages

   - Linearity is broken below 30 keV (residual >10% below 30 keV)
   - At 30 keV, the FWHM energy resolution of GAGG:Ce (40%) is poorer than that of CsI:Tl (32%)
   - Prominent lines appear due to proton activation (e.g., 511 keV)
   - Light amount of afterglow is larger than those for other scintillators (the afterglow-to-scintillation-light ratio is ~4%)
   - The afterglow decay time is long (approximately 1 day is required to return to the original background level)

GAGG:Ce has weak temperature dependence and high radiation tolerance; therefore, this material has potential for effective use in the space environment, which features a wide temperature range. However, on the other hand, certain problems are associated with GAGG:Ce, such as decreased light yield at low energy, the existence of the prominent 511-keV line due to proton activation, and an afterglow. Regarding the afterglow of GAGG:Ce, we showed that it can be improved by Mg doping (section 4.7). Considering the advantages and disadvantages of Mg doping, the Mg doping fractions should be optimized in accordance with the given application. Nonetheless, our measurements of the afterglow emission spectra elucidate the origin of the afterglow mechanism. In this respect, further detailed study of GAGG:Ce is both necessary and important for future development of radiation detectors.

Acknowledgments

This work was supported by JSPS KAKENHI, Grant Number JP15H05720.

2018 JINST 13 P02023

A Properties of inorganic scintillators

Table 5. Properties of inorganic scintillators [16, 29, 30, 34, 35, 38, 39, 47, 59, 61–80].

	NaI:Tl	CsI:Tl	BGO	GSO	YAG	LuAG	LYSO	GAGG:Ce
Composition	NaI:Tl	CsI:Tl	$Bi_4Ge_3O_{12}$	Gd_2SiO_5	$Y_3Al_5O_{12}$	$Lu_3Al_5O_{12}$	$Lu_{1.8}Y_{0.2}SiO_5$	$Gd_3(Ga, Al)_5O_{12}$
Density [g/cm^3]	3.67	4.51	7.13	6.71	4.56	6.70	7.10	6.63
Light yield [photon/MeV]	38,000	65,000	8,200	9,000	17,000	12,500	30,000	56,000
Emission wavelength [nm]	415	540	480	440	550	390	420	520
Decay time [ns][1]	230	680	300	60	90	10	45	100
Light-yield temperature dependence [%][2]	~20	~20	~50	~30	~10	~10	~1[3]	~20
Decay-time temperature dependence [%][4]	~40	~50	~70	~15[5]	–	–	–	12
Changes in light yield due to radiation damage [%][6]	–	20–70	10–40	~10	–	~10	–	~10
Hygroscopic	yes	slightly	no	no	no	no	no	no

[1]At 20 °C. [2]Comparison of light yields at −20 and 20 °C. [3]Comparison of light yields at 15 and 25 °C. [4]Comparison of scintillation decay times at −40 and 40 °C.
[5]Comparison of light yields at 25 and 125 °C. [6]100-krad gamma-rays

B Estimation of activation background in satellite environment

Based on the results for the detector background induced by the proton activation discussed in section 3.1, we can calculate the expected background in space. Figure 24 shows the calculated backgrounds 24 h and 1 y after launch, assuming LEO with an inclination angle of 31°, a 575-km altitude, and 96.2-min orbital period, which is the same as that of ASTRO-H (also known as "Hitomi") [33]. In this case, the scintillator enters the SAA five times per day and the corresponding features appear as five distinct peaks in figure 24. This brief calculation would be useful for a quantitative estimate of detector sensitivity using the GAGG:Ce.

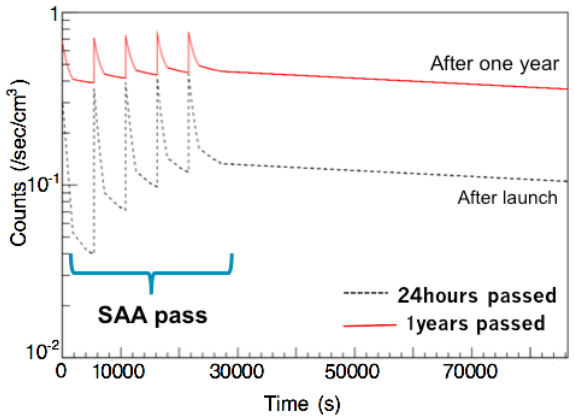

Figure 24. Estimated activation background of GAGG:Ce in LEO.

C Half-life results obtained from proton-beam irradiation experiment

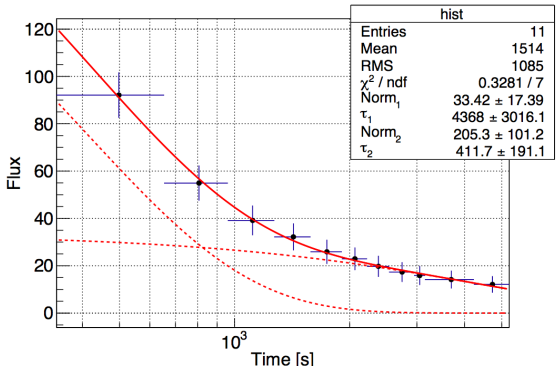

Figure 25. 102-keV source.

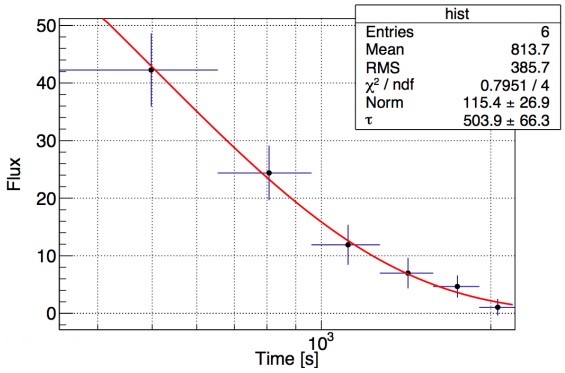

Figure 26. 220-keV source.

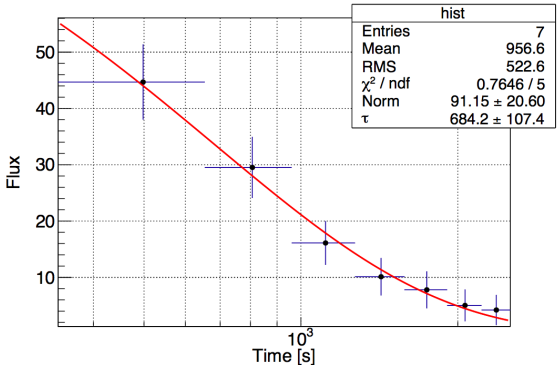

Figure 27. 333-keV source.

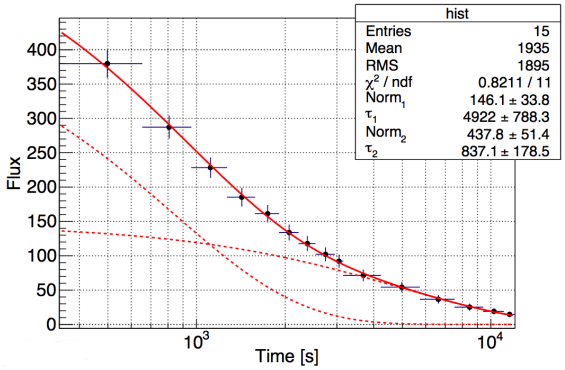

Figure 28. 511-keV source.

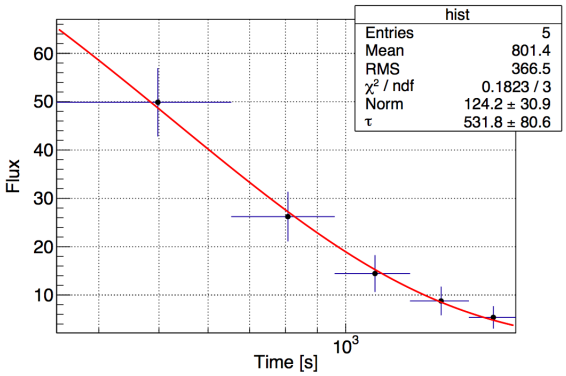

Figure 29. 629-keV source.

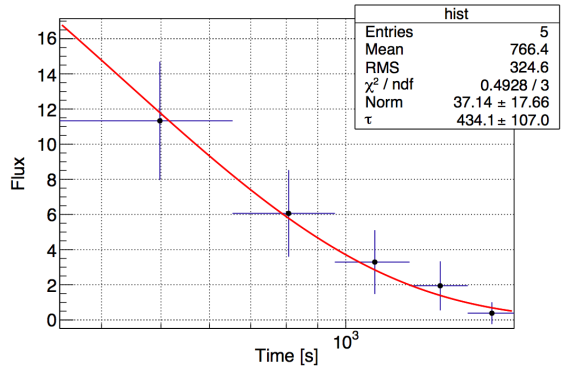

Figure 30. 784-keV source.

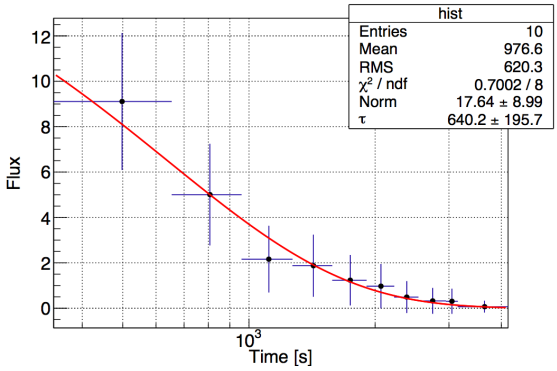

Figure 31. 871-keV source.

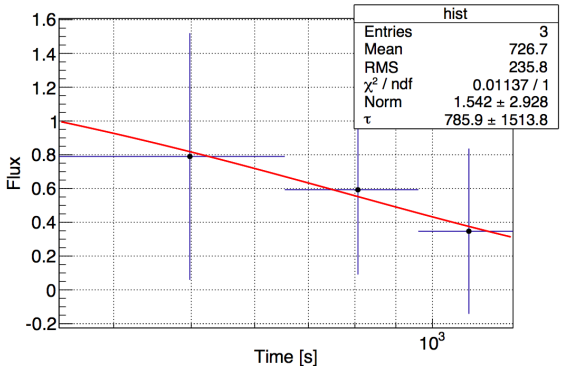

Figure 32. 993-keV source.

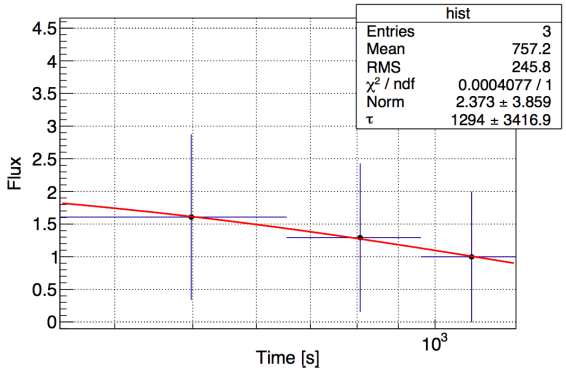

Figure 33. 1038-keV source.

References

[1] A.P.A. Rodnyi, *Physical Processes in Inorganic Scintillators*, CRC Press (1997).

[2] K. Kamada et al., *2 inch diameter single crystal growth and scintillation properties of* $Ce{:}Gd_3Al_2Ga_3O_{12}$, *J. Cryst. Growth* **352** (2012) 88.

[3] A. Kishimoto et al., *Development of a compact scintillator-based high-resolution Compton camera for molecular imaging*, *Nucl. Instrum. Meth. A* **845** (2017) 656.

[4] S. Yamamoto et al., *Development of a high resolution gamma camera system using finely grooved GAGG scintillator*, *Nucl. Instrum. Meth. A* **821** (2016) 28.

[5] M. Arimoto et al., *Development of the hard x-ray monitor onboard WF-MAXI*, *Proc. SPIE* **9144** (2014) 91445Z

[6] A. Kishimoto et al., *First demonstration of multi-color 3-D in vivo imaging using ultra-compact camera*, *Sci. Rept.* **7** (2017) 2110.

[7] M. Arimoto et al., *Development of a 32-channel ASIC for an X-ray APD detector onboard the ISS*, *Nucl. Instrum. Meth.* **A 882** (2017) 138.

[8] J. Kataoka et al., *Handy Compton camera using 3D position-sensitive scintillators coupled with large-area monolithic MPPC arrays*, *Nucl. Instrum. Meth.* **A 732** (2013) 403.

2018 JINST 13 P02023

[9] Y. Iwamoto et al., *Novel methods for estimating 3D distributions of radioactive isotopes in materials*, *Nucl. Instrum. Meth.* **A 831** (2016) 295.

[10] T. Oshima et al., *Development of a high-precision color gamma-ray image sensor based on TSV-MPPC and diced scintillator arrays*, *Nucl. Instrum. Meth.* **A 803** (2015) 8.

[11] W.N. Johnson et al., *The oriented scintillation spectrometer experiment: instrument description*, *Astrophys. J. Suppl.* **86** (1993) 693.

[12] W.N. Johnson et al., *Initial results from OSSE on the Compton Observatory*, *Astron. Astrophys. Suppl. Ser.* **97** (1993) 21.

[13] R.E. Rothschild et al., *In-flight performance of the high energy X-ray timing experiment on the rossi X-ray timing explorer*, *Astrophys. J.* **496** (1998) 538.

[14] S.B. Gavler et al., *Radiation tests of CsI(Tl) crystals for the GLAST satellite mission*, *Nucl. Instrum. Meth.* **A 545** (2005) 842.

[15] K. Hurley, *Phosphorescence in CsI Crystall*, *Astron. Astrophys.* **69** (1978) 313.

[16] I. Chakin et al., *Radiation hardness study of CsI(Tl) scintillation crystals for the Belle II calorimeter*, 2017 *JINST* **12** C06034.

[17] C. Delaney and A. Lamki, *Long-Lived phosphorescent Components in NaI(Tl) and CsI(Tl)*, *Int. J. Appl. Radiat. Isot.* **19** (1968) 169.

[18] S. Koicki et al., *The investigation of the 0.15s phosphorescent of NaI(Tl) and its application in scintillation counting*, *Nucl. Instrum. Meth.* **108** (1973) 297.

[19] C. Brecher et al., *Time-resolved studies of the nonexponential decay of CsI(Tl) after short-pulse X-ray excitation*, *Nucl. Instrum. Meth.* **A 537** (2005) 117.

[20] S. Thacker et al., *Low-afterglow CsI:Tl microcolumnar films for small animal high-speed microCT*, *Nucl. Instrum. Meth.* **A 604** (2009) 89.

[21] M.E. Casey et al., *A multicrystall two dimensinal bgo detector system for positron emission tomography*, *IEEE Trans. Nucl. Sci.* **33** (1986) 460.

[22] W.-H. Wong et al., *An Analog Decoding BGO Block Detector Using Circular Photomultipliers*, *IEEE Trans. Nucl. Sci.* **42** (1995) 1095.

[23] S. Yamamoto, *A dual layer DOI GSO block detector for a small animal PET*, *Nucl. Instrum. Meth.* **A 598** (2009) 480.

[24] Y. Uchiyama et al., *Study of Energy Response of Gd_2SiO_5:Ce^{3+} Scintillator for the ASTRO-E Hard X-Ray Detector*, *IEEE Trans. Nucl. Sci.* **48** (2001) 379.

[25] P. Ubertini et al., *The IBIS telescope on board integral*, in *The Transparent Universe*, Vol. 382, ESA Special Publication (1997), p. 599.

[26] M. Kokubun et al., *Activation of the ASTRO-E Hard X-ray Detector in Low Earth Orbit*, *IEEE Nucl. Sci. Symp. Med. Imag. Conf.* **1** (1998) 227.

[27] M. Sakano et al., *Estimating the radiative activation characteristics of a $Gd_3Al_2Ga_3O_{12}$:Ce scintillator in low earth orbit*, 2014 *JINST* **9** P10003.

[28] P.R. Truscott et al., *Comparison of Activation Effects in y-ray Detector Materials*, *IEEE Nucl. Sci. Symp. Med. Imag. Conf.* **1** (1995) 38.

[29] G.F. Knoll, *Radiation Detection and Measurement*, 4th edition, Ohmsha LTD (2013).

2018 JINST 13 P02023

[30] M. Tanaka et al., *Applications of cerium-doped gadolinium silicate Gd_2SiO_5:Ce scintillator to calorimeters in high-radiation environment*, *Nucl. Instrum. Meth.* **A 404** (1998) 283.

[31] M. Tashiro et al., *Performance of the ASTRO-E Hard X-Ray Detector*, *IEEE Trans. Nucl. Sci.* **49** (2002) 1893.

[32] A. von Kienlin et al., *A GRB Detection System using the BGO-Shield of the INTEGRAL-Spectrometer SPI*, astro-ph/0109119.

[33] T. Takahashi et al., *The ASTRO-H X-ray astronomy satellite*, *Proc. SPIE* **9144** (2014) 914425 [arXiv:1412.1356].

[34] C. Melcher, *Scintillators for well logging applications*, *Nucl. Instrum. Meth.* **B 40** (1989) 1214.

[35] N. Tsuchida et al., *Temperature dependence of gamma-ray excited scintillation time profile and light yield of GSO, YSO, YAP and BGO*, *Nucl. Instrum. Meth.* **A 385** (1997) 290.

[36] J. Iwanowska et al., *Performance of cerium-doped $Gd_3Al_2Ga_3O_{12}$ (GAGG:Ce) scintillator in gamma-ray spectrometry*, *Nucl. Instrum. Meth.* **A 712** (2013) 34.

[37] O. Sakthong et al., *Scintillation properties of $Gd_3Al_2Ga_3O_{12}$:Ce^{3+} single crystal scintillators*, *Nucl. Instrum. Meth.* **A 751** (2014) 1.

[38] J.D. Valentine et al., *Temperature dependence of CSl(TI) gamma-ray excited scintillation characteristics*, *Nucl. Instrum. Meth. A* **325** (1993) 147.

[39] W.J.V. Sciver et al., *Fundamental Studies of Scintillation Phenomena in NaI*, *IRE Trans. Nucl. Sci.* **5** (1958) 90.

[40] G. Weidenspointner et al., *Positron astronomy with SPI/INTEGRAL*, *New Astron. Rev.* **52** (2008) 454.

[41] G. De Cesare, *Searching for the 511 keV annihilation line from galactic compact objects with the IBIS gamma ray telescope*, *Astron. Astrophys.* **531** (2011) A56.

[42] J.A.E. Agency, *Table of Nuclear Data*, Nuclear Data Center, http://wwwndc.jaea.go.jp/NuC/index.html.

[43] T.J.R. Association, *Table of isotope*, Ohmsha LTD (2013).

[44] S. Luz Maria Martines, *Analysis of LEO Radiation Environment and its Effects on Spacecraft's Critical Electronic Devices*, https://commons.erau.edu/edt/102.

[45] O. Zeynali et al., *The design and simulation of the shield reduce ionizing radiation effects on electronic circuits in satellites*, *Electr. Electron. Eng.* **1** (2011) 112.

[46] J. Kataoka et al., *Expected radiation damage of reverse-type APDs for the Astro-H mission*, 2012 *JINST* **7** P06001.

[47] S. Longo et al., *Radiation Hardness of 30 cm Long CsI(Tl) Crystals*, 2016 *JINST* **11** P08017 [arXiv:1608.07556].

[48] Belle collaboration, S.K. Sahu et al., *Radiation hardness of undoped BGO crystals*, *Nucl. Instrum. Meth.* **A 388** (1997) 144.

[49] M. Mori et al., *Comparative study of optical and scintillation properties of Ce:YAGG, Ce:GAGG and Ce:LuAGG transparent ceramics*, *J. Ceramic Soc. Jpn.* **124** (2016) 569.

[50] A. Satoh et al., *Time-resolved photoluminescence spectroscopy of Ce:$Gd_3Al_2Ga_3O_{12}$ crystals*, *Jpn. J. Appl. Phys.* **53** (2014) 05FK01.

[51] M. Kitaura et al., *Probing shallow electron traps in cerium-doped Gd3Al2Ga3O12 scintillators by UV-induced absorption spectroscopy*, *Appl. Phys. Express* **9** (2016) 072602.

2018 JINST 13 P02023

[52] M. Nikl et al., *Luminescence and scintillation mechanism in Ce^{3+} and Pr^{3+} doped $(Lu,Y,Gd)_3(Ga,Al)_5O_{12}$ single crystal scintillators*, Physica Status Solidi **10** (2013) 172.

[53] K. Kamada et al., *Mg co-doping effects on Ce doped $Y_3(Ga,Al)_5O_{12}$ scintillator*, IOP Conf. Ser. **169** (2017) 012013.

[54] E. Mihokova et al., *Deep trapping states in cerium doped $(Lu,Y,Gd)_3(Ga,Al)_5O_{12}$ single crystal scintillators*, Radiat. Meas. **56** (2013) 98.

[55] V. Babin et al., *Effect of Mg^{2+} ions co-doping on luminescence and defects formation processes in $Gd_3(Ga,Al)_5O_{12}$:Ce single crystals*, Opt. Mater. **66** (2017) 48.

[56] K. Kamada et al., *Development of a Prototype Detector Using APD-Arrays Coupled With Pixelized Ce:GAGG Scintillator for High Resolution Radiation Imaging*, IEEE Trans. Nucl. Sci. **61** (2014) 348.

[57] M. Kitaura et al., *Phosphorescence of Ce-doped $Gd_3Al_2Ga_3O_{12}$ crystals studied using luminescence spectroscopy*, J. Appl. Phys. **115** (2014) 083517.

[58] K. Kamada et al., *Large Size Czochralski Growth and Scintillation Properties of Mg^{2+} Co-doped $Ce : Gd_3Ga_3Al_2O_{12}$* IEEE Trans. Nucl. Sci. **63** (2016) 443.

[59] K. Kamada et al., *Alkali earth co-doping effects on luminescence and scintillation properties of Ce doped $Gd_3Al_2Ga_3O_{12}$ scintillator*, Opt. Mater. **41** (2015) 63.

[60] M. Lucchini et al., *Effect of Mg^{2+} ions co-doping on timing performance and radiation tolerance of Cerium doped $Gd_3Al_2Ga_3O_{12}$ crystals*, Nucl. Instrum. Meth. **A 816** (2016) 176.

[61] M.T. Lucchini et al., *Timing capabilities of garnet crystals for detection of high energy charged particles*, Nucl. Instrum. Meth. **A 852** (2017) 1.

[62] M. Moszynski et al., *Absolute Light Output of Scintillators*, IEEE Trans. Nucl. Sci. **44** (1997) 1052.

[63] D.W. Aitken et al., *The fluorescent response of NaI(Tl), CsI(Tl), CsI(Na; and CaF_2(Eu) to X-rays and low energy gamma rays*, IEEE Trans. Nucl. Sci. **14** (1967) 468.

[64] Crystal Saint-Gobain Co., *BGO bismuth germanate scintillation material*, https://www.crystals.saint-gobain.com/sites/imdf.crystals.com/files/documents/bgo-material-data-sheet_69763.pdf.

[65] S. Belogurov, G. Bressi, G. Carugno and Yu. Grishkin, *Properties of Yb-doped scintillators: YAG, YAP, LuAG*, Nucl. Instrum. Meth. **A 516** (2004) 58.

[66] S. Gridin et al., *Scintillation properties of CsI:In single crystals*, Nucl. Instrum. Meth. **A 761** (2014) 13.

[67] M. Moszynski, T. Ludziejewski, D. Wolski, W. Klamra and L.O. Norlin, *Properties of the YAG : Ce scintillator*, Nucl. Instrum. Meth. **A 345** (1994) 461.

[68] J.T.M. de Haas et al., *Advances in Yield Calibration of Scintillators*, IEEE Trans. Nucl. Sci. **55** (2008) 1086.

[69] W.W. Moses et al., *$LuAlO_3$:Ce — A high density, high speed scintillator for gamma detection*, IEEE Trans. Nucl. Sci. **42** (1995) 275.

[70] T. Bhattacharjee et al., *Comparative studies of YAG(Ce) and CsI(Tl) scintillators*, Nucl. Instrum. Meth. **A 484** (2002) 364.

[71] T.K. Lewellen, *Recent developments in PET detector technology*, Phys. Med. Biol. **53** (2008) R287.

[72] K.D. Ianakiev, B.S. Alexandrov, P.B. Littlewood and M.C. Browne, *Temperature behavior of NaI (Tl) scintillation detectors*, Nucl. Instrum. Meth. **A 607** (2009) 432 [physics/0605248].

2018 JINST 13 P02023

[73] Crystal Saint-Gobain Co., *Csi(tl), Csi(na) cesium iodide scintillation material*, https://www.crystals.saint-gobain.com/sites/imdf.crystals.com/files/documents/csitl-and-na-material-data-sheet.pdf.

[74] W. Wolszczak et al., *Temperature Properties of Scintillators for PET Detectors: a Comparative Study*, *IEEE Nucl. Sci. Symp. Med. Imag. Conf.* (2014) 1.

[75] H. Takahashi et al., *The Temperature Dependence of Gamma-ray Responses of YAG:Ce Ceramic Scintillators*, *IEEE Nucl. Sci. Symp. Conf. Rec.* **3** (2005) 1337.

[76] T. Iwashita et al., *Radiation Hardness Test of Pr:LuAG and BSO scintillators*, IEEE Nuclear Science Symposuim Medical Imaging Conference, 2010, pp. 278–279. doi:. *IEEE Nucl. Sci. Symp. Med. Imag. Conf.* (2010) 278.

[77] R. Mao et al., *Optical and Scintillation Properties of Inorganic Scintillators in High Energy Physics*, *IEEE Nucl. Sci. Symp. Conf. Rec.* **3** (2007) 2285.

[78] W. Drozdowski et al., *Scintillation Properties of Praseodymium Activated $Lu_3Al_5O_{12}$ Single Crystals*, *IEEE Trans. Nucl. Sci.* **55** (2008) 2420.

[79] S. Kurosawa et al., *Temperature dependence of the scintillation properties of Ce:GSO and Ce:GSOZ*, *Nucl. Instrum. Meth. A* **690** (2012) 53.

[80] Crystal Saint-Gobain Co., *Lyso scintillation material*, https://www.crystals.saint-gobain.com/sites/imdf.crystals.com/files/documents/lyso-material-data-sheet_0.pdf.

2018 JINST 13 P02023